Title: Significance of extended N-terminal region and a first motif residue in a third transmembrane helix of a novel pump-like cation channelrhodopsin HulaCCR

Authors:

Shunki Takaramoto[1], Shai Fainsod[2], Takashi Nagata[1], Andrey Rozenberg[2], Oded Béjà[2,3], Keiichi Inoue[1].*

Affiliations:

1. The Institute for Solid State Physics, The University of Tokyo, Kashiwa, Chiba 277-8581, Japan
2. Faculty of Biology, Technion — Israel Institute of Technology, Haifa 3200003, Israel
3. The Nancy and Stephen Grand Technion Energy Program (GTEP), Technion—Israel Institute of Technology, Haifa 3200003, Israel

Corresponding author:

Correspondence to Keiichi Inoue. E-mail: inoue@issp.u-tokyo.ac.jp; telephone: +81-4-7136-3230; postal address: Room A401, The Institute for Solid State Physics, The University of Tokyo, 5-1-5, Kashiwanoha, Kashiwa, Chiba 277-8581, Japan.

Abstract

Microbial rhodopsins are a family of photoreactive membrane proteins that have seven transmembrane helices and a retinal chromophore. Among them, channelrhodopsins are light-induced ion channels making them popular tools for modulating neuronal activity in optogenetics. Cation channelrhodopsins (CCRs), first recognized as the main photoreceptors in the model

chlorophyte *Chlamydomonas reinhardtii*, have since been identified in diverse species of green algae, as well in other unicellular eukaryotes. The CCRs from non-chlorophyte species are commonly referred to as the bacteriorhodopsin-like channelrhodopsins, or BCCRs, as most of them feature the three characteristic amino acid residues of the "DTD motif" in the third transmembrane helix (TM3 or helix C) matching the canonical DTD motif of the well-studied archaeal light-driven proton pump bacteriorhodopsin. Here, we report characterization of HulaCCR, a novel BCCR identified through metatranscriptomic analysis of a unicellular eukaryotic community in Lake Hula, Israel. Interestingly, HulaCCR has an ETD motif in TM3 in which the first residue of the canonical motif is substituted for glutamate. Electrophysiological measurements of the wild-type and a mutant with a DTD motif of HulaCCR suggest the critical role of the first glutamate in spectral tuning and gating. Additionally, HulaCCR exhibits long extensions at the N- and C-termini. Photocurrents recorded from a truncated variant without the signal peptide predicted at the N-terminus were diminished, and membrane localization of the truncated variant significantly decreased, which indicates that the signal peptide is important for membrane trafficking of HulaCCR. These characteristics of HulaCCR would be related to a new biological significance in the original unidentified species, distinct from those known for other BCCRs.

Introduction

Microbial rhodopsins are a family of photoreactive membrane proteins that have seven transmembrane helices and a retinal chromophore covalently binding to a conserved lysine residue in the 7th transmembrane helix (called TM7 or helix G).[1–3] Among them, channelrhodopsins (ChRs) are light-induced ion channels and are extensively utilized in optogenetics.[4,5] Channelrhodopsins were first discovered in green algae when the photoreceptors responsible for phototactic behavior in *Chlamydomonas reinhardtii* were identified as microbial rhodopsin

channels transporting cations, or cation channelrhodopsins (CCRs).[6–8] In contrast to *Chlamydomonas*, two different types of ChRs were subsequently identified in the cryptophyte *Guillardia theta*: a distinct family of CCRs, as well as a family of anions-transporting ChRs, or anion channelrhodopsins (ACRs), which was the first indication of the high diversity of ChRs among unicellular eukaryotes.[9,10] Natural and modified CCRs and ACRs have since been used as molecular tools in optogenetic research to stimulate or inhibit neuronal firing by light, respectively.[11–14]

Many microbial rhodopsins, including the well-characterized light-driven proton pump bacteriorhodopsin from *Halobacterium salinarum* (*Hs*BR), feature three characteristic amino acid residues together constituting the canonical "DTD motif" in the third transmembrane helix (called TM3 or helix C). This motif is composed of two aspartic acid residues and a threonine residue: D85/D96 and T89 in *Hs*BR, respectively.[15] One remarkable feature of the cryptophyte CCRs from *Guillardia theta* was the presence of the DTD motif identical to that of *Hs*BR.[16,17] Following the discovery of the CCRs from *G. theta*, many CCRs possessing the DTD or similar motifs were found in other species, collectively referred to as the bacteriorhodopsin-like channelrhodopsins (BCCRs). Among them, ChRmine from the cryptophyte *Rhodomonas lens* exhibiting high photocurrents and high light sensitivity has emerged as the model BCCR and has found its application in deep transcranial optogenetics.[18–20] Recent years have also witnessed the discovery of highly potassium selective BCCRs, the kalium channelrhodopsins (KCRs) from the stramenopiles *Hyphochytrium catenoides* (*Hc*KCR1 and *Hc*KCR2)[21] and *Wobblia lunata* (WiChR)[22], as well as other heterotrophic flagellates. Since KCRs efficiently induce hyperpolarization by K^+ efflux, they are used for precise optogenetic inhibition.

Here, we characterize HulaCCR, a novel microbial rhodopsin identified through metatranscriptomic analysis of the unicellular eukaryotic community of Lake Hula, Israel. This

rhodopsin has an ETD motif in TM3 and belongs to the family of stramenopile CCRs which includes KCRs and other CCRs from cultured heterotrophic flagellates and environmental sources [22, 23] (Figs. 1a and b). While uncommon among BCCRs, the ETD motif is not an idiosyncrasy of HulaCCR and is found in the related proteins mgCCR1[23] and P1ChR1[22]. The structure of HulaCCR predicted with AlphaFold2 Colab [24] features an unusually long N-terminal extension with a signal peptide and a prominent partially structured long C-terminal extension (Fig. 1b).

In this study, we investigated the function of HulaCCR using electrophysiological techniques. As a result, it was revealed that this rhodopsin exhibits non-specific cation channel activity. To understand the role of the substitution of glutamate for the ancestral aspartate at the first position of the TM3 motif in HulaCCR, we examined the effects of this residue on the channel activity. In addition, we investigated the role of the long extensions at the N- and C-termini of HulaCCR.

Results

Identification of HulaCCR

HulaCCR was identified as part of an ongoing metatranscriptomic study of the unicellular eukaryotic community of Lake Hula in Northern Israel. This protein was chosen as a representative of a BCCR clade abundant in the Hula assembly and to which the partially characterized ChRs mgCCR1–3[23] also belong (Figs. 1a and b). Ideal for the study of the role of the carboxylate amino acid at the first position of the TM3 motif, this clade demonstrates both DTD and ETD variants, with mgCCR1 and HulaCCR having the otherwise uncommon glutamate. HulaCCR and mgCCR1 are the closest relatives, with a modest overall pairwise sequence identity of 48%, least similar in the N-terminal extension. The identity of the organism possessing these ChRs remains unknown.

97 **Ion transport activity of HulaCCR**

98 Upon establishing the expression of HulaCCR in COS-1 cells, we investigated the absorption
99 spectra of the protein solubilized from the membrane fraction of the cells with a solution containing
100 n-dodecyl-β-D-maltoside (DDM). The absorption maximum wavelength (λ_{max}) of HulaCCR was
101 determined to be 545 nm by a hydroxyl amine (HA) bleaching method[25] (Fig. 1c). To investigate
102 the molecular function of HulaCCR, electrophysiological measurements were conducted. Based on
103 the strong EYFP fluorescence on the outlines of transfected cultured cells, we determined that
104 HulaCCR was well expressed in the plasma membrane (Fig. 1d). Whole-cell patch clamp
105 recordings were performed using these cells. With standard pipette ([K^+] = 128 mM) and
106 extracellular ([Na^+] = 142 mM) solutions, a significant photocurrent appeared upon illumination
107 with 542-nm light (Fig. 1e). The photocurrent depended on the holding potential and exhibited an
108 inversion from positive to negative currents along with increasing the holding potential from −80
109 to 60 mV, indicating that HulaCCR exhibits light-dependent ion channel activity. Changing the
110 cations in both the patch pipette and extracellular solutions to N-methyl-D-glucamine (NMG)
111 resulted in a profound decrease in photocurrent intensity (Fig. 1e, right). Furthermore, in this
112 measurement, despite the anion conditions being asymmetric between the external and internal side
113 of the membrane, where the pipette and extracellular solutions contained 90 mM glutamate and
114 151 mM Cl^-, respectively, the reversal potential remained at around 0 mV, excluding the possibility
115 of anion channel activity and indicating H^+ channel activity. We conclude that HulaCCR possesses
116 cation channel transport activity.

117 Next, to investigate the ion selectivity of HulaCCR, photocurrents were measured in
118 extracellular solutions containing different cations (Fig. 2a), and current–voltage (*I–V*) curves were
119 plotted based on peak current intensities (Fig. 2b). The *I–V* curves were fitted by a quadratic
120 function, then the reversal potentials (E_{rev}) of the photocurrents were estimated. Taking the results

with NMG-containing extracellular solution as a reference, the reversal potential shift (ΔE_{rev}) was calculated. ΔE_{rev} values increased with monovalent cations, while only low values were observed with divalent cations, Mg^{2+} and Ca^{2+}. Hence, Mg^{2+} and Ca^{2+} hardly permeate through the channel pore in HulaCCR. Assuming that only monovalent cations in the extracellular/pipette solutions permeate, the relative cation permeability (P_{X+}/P_{H+}) was calculated using Goldman–Hodgkin–Katz (GHK) equation (eq. 1) from ΔE_{rev} values,

$$\Delta E_{\mathrm{rev}} = \frac{RT}{F} ln \left(\frac{P_{\mathrm{X}}[\mathrm{X}^+]_{\mathrm{o}} + P_{\mathrm{H}}[\mathrm{H}^+]_{\mathrm{o}}}{P_{\mathrm{H}}[\mathrm{H}^+]_{\mathrm{o}}}\right), \quad (1)$$

where R is the gas constant, T is the temperature, and F is the Faraday constant. The obtained values P_{X+}/P_{H+} are shown in Fig. 2c. P_{Mg2+}/P_{H+} and P_{Ca2+}/P_{H+} were not determined by GHK flux equation[26] for divalent cations at equilibrium (eq. 2) because the calculated values of P_{Mg2+}/P_{H+} and P_{Ca2+}/P_{H+} were considerably smaller than the experimental error.

$$4P_{\mathrm{Mg}} \frac{[\mathrm{Mg}^{2+}]_{\mathrm{i}} exp\left(\frac{2E_{\mathrm{rev}}F}{RT}\right) - [\mathrm{Mg}^{2+}]_{\mathrm{o}}}{1 - exp\left(\frac{2E_{\mathrm{rev}}F}{RT}\right)} + 4P_{\mathrm{Ca}} \frac{[\mathrm{Ca}^{2+}]_{\mathrm{i}} exp\left(\frac{2E_{\mathrm{rev}}F}{RT}\right) - [\mathrm{Ca}^{2+}]_{\mathrm{o}}}{1 - exp\left(\frac{2E_{\mathrm{rev}}F}{RT}\right)} + P_{\mathrm{H}} \frac{[\mathrm{H}^+]_{\mathrm{i}} exp\left(\frac{E_{\mathrm{rev}}F}{RT}\right) - [\mathrm{H}^+]_{\mathrm{o}}}{1 - exp\left(\frac{E_{\mathrm{rev}}F}{RT}\right)} = 0$$

(2)

From these results, it can be concluded that HulaCCR exhibits a strong ion selectivity for monovalent cations, and this property is similar to those of *Gt*CCR4[27] and ChRmine[28]. Moreover, there was not much difference in the selectivity among monovalent alkali metal cations (Fig. 2c).

Mutational analysis of spectral tuning and gating kinetics in HulaCCR

Many BCCRs share the DTD motif in TM3 identical to the residues D85, T89, and D96 of *Hs*BR. As mentioned above, in HulaCCR, a glutamate (E176) is present at the position of the first motif residue, forming an ETD motif (Fig. 1a). To investigate the roles of the amino acid residues near the retinal chromophore, including E176 (Fig. 3a), photocurrents of several single mutants were

144 measured (Figs. 3b–e and S2). While the E176D mutant, in which the DTD motif is restored,
145 exhibited photocurrents similar to those of the wild-type protein (WT), its action spectrum slightly
146 blue-shifted compared to the WT spectrum (Fig. 3b), indicating the red-shifting spectral-tuning
147 effect of E176 in HulaCCR. To determine whether this residue is crucial for channel gating,
148 photocurrents were measured with a higher time resolution using nanosecond-pulsed laser flashes
149 (Fig. 3c). The time course of photocurrents due to channel opening and closing was reproduced
150 with a quadruple-exponential function. The obtained time constants were shown in Fig. 3d. Notably,
151 the closing rate of outward current in E176D was significantly slower compared to that of the WT,
152 suggesting the importance of E176 in the closing kinetics.

153 In chlorophyte channelrhodopsins and BCCRs, a cysteine residue is conserved at the position
154 corresponding to T90 in *Hs*BR in TM3 (Fig. 1a). This cysteine together with D156 in TM4
155 constitutes the "DC gate" in *Cr*ChR2 [29], and HulaCCR mutants in which C181 were substituted
156 with alanine or serine (C181A and C181S) exhibited significantly slower channel closing after 200-
157 ms illumination (Fig. S2d). Both mutants showed a highly prolonged channel closing rate in the
158 nanosecond-pulse excitation experiments, as observed in cysteine mutants of other
159 channelrhodopsins (Fig. 3e).[30,31]

160 Next, we attempted to tune the spectrum of HulaCCR by mutating amino acid residues near
161 the retinal chromophore. First we noticed that HulaCCR has C303 adjacent to K304 that forms the
162 Schiff-base linkage with the retinal chromophore in TM7, a trait shared most notably with the
163 KCRs (Figs. 3a, S1),[21] while most of the other BCCRs have alanine at this position similarly to
164 *Hs*BR. Importantly, in the case of *Cr*ChR2, substituting alanine for serine at this position causes a
165 red shift in the absorption spectrum.[32] Nevertheless, the action spectrum of the photocurrents of
166 the HulaCCR C303A mutant showed no significant red shift compared to the WT (Fig. S2c). Taking
167 a different approach, we attempted to introduce negative charges on the β-ionone ring side of the

168 retinal which is known to stabilize the electronically excited state, thus leading to a red shift in the
169 absorption spectrum.[33] Hence, the action spectra of mutants of residues shown in Fig. S2b,
170 L208M, A232C, A232S, and P276T were measured. This strategy did result in significantly red-
171 shifted action spectra compared to that of the WT (Fig. S2c).

172 Although the expected spectral shift did not occur in C303A, we found a significant difference
173 in other photocurrent behaviors in this mutant. The decay rate of photocurrents after light-off in
174 C303A was slower compared to that of the WT (Fig. S2a). The slower channel closing might be
175 the result of a slower photocycle, as seen for example in DC-gate mutants of *Cr*ChR2.[30,34] The
176 dependence of photocurrent intensity on excitation light power was also investigated under
177 continuous light illumination. In this case, it is anticipated that for channelrhodopsins with slower
178 photoreaction cycles, the photocurrent intensity will saturate at a lower light intensity compared to
179 those with faster photocycles. Hence, photocurrent intensities for the WT and C303A were
180 measured during continuous light illumination for 100 ms and were plotted against power density
181 of the excitation light (Fig. 3f). As a result, the C303A mutant with the slower channel closing rates
182 exhibited a lower EC_{50} value than that of the WT. Additionally, when compared to another BCCR,
183 ChRmine, which has a slower closing rate than that of the HulaCCR WT (Fig. S2a), the trend that
184 longer closing rates lead to lower EC_{50} values was maintained (Fig. 3f).

185 Previous studies on BCCRs suggested that amino acid residues on the intracellular side are
186 also crucial for the gating mechanism. In *Gt*CCR2, a mutant in which D98 (equivalent to D96 in
187 *Hs*BR) in TM3 was mutated to asparagine showed no significant channel current.[35] The effect
188 of the identical mutation has been investigated in other BCCRs, including ChRmine[28] and
189 *Hc*KCR1[36], where the motif residues DTD are changed to DTN. It resulted in a decrease in cation
190 channel activity. Moreover, it has been previously suggested for *Gt*CCR2 that proton transfer from
191 D98 (corresponding to D96 in BR) to an unknown cytoplasmic residue and back govern the

192 opening and closing of the channel, respectively.[35] We notice that BCCRs have characteristic
193 well-conserved acidic amino acids on the C-terminal side of TM7 (Fig. S1). We thus hypothesized
194 that a potential proton exchange between the third motif residue (D) in TM3 and acidic amino acid
195 residues at the cytoplasmic side of TM7 in BCCRs plays a critical role in the channel gating. To
196 test this hypothesis, we generated mutants corresponding to these residues in HulaCCR: D187N in
197 TM3, and E319Q, D320N, and E322Q, in TM7, and analyzed their photocurrents (Figs. S3a–c).
198 The D187N and D320N mutants exhibited low expressions in the plasma membrane probably due
199 to a significant decrease in protein stability, resulting in no observable photocurrents (Fig. S3c).
200 Whereas E319Q exhibited photocurrent intensity and opening/closing rates similar to that of the
201 WT (Figs. S3b and c), a decrease in the closing rate after 200-ms illumination was indeed observed
202 for E322Q (17 ± 2 ms, 15 ± 1 ms, and 38 ± 2 ms for the WT, E319Q, and E322Q at −60 mV holding
203 potential, respectively, $n = 5$, Fig. S3b).

204 Next we compared photocurrent signals upon nanosecond laser-pulse illumination to precisely
205 determine the difference in the time constants of opening and closing (Figs. S3d and e).
206 Additionally, to clarify the relationship between the proton transfer reaction and channel dynamics,
207 the kinetic isotope effect (KIE) in heavy water (D_2O) was investigated by calculating a ratio
208 between the time constants with D_2O and H_2O solutions with respect to the channel opening and
209 closing kinetics. If a proton transfer is the rate-limiting elementary reaction step, the reaction rate
210 decreases in D_2O, thereby exhibiting a significant KIE value.[37–39] For the HulaCCR WT and
211 E322Q, the time courses of photocurrents at membrane potentials of −60 mV and 40 mV are shown
212 in Fig. S3d. The photocurrent kinetic traces of E322Q were fitted with a quadruple-exponential
213 function, similar to the WT, to determine the time constants of channel opening and closing (Fig.
214 S3e). By calculating the ratio of closing time constants in D_2O to those in H_2O, the KIE was
215 determined to be 1.61 ± 0.06 for the WT and 1.18 ± 0.03 for E322Q, respectively. Hence, E322Q

216 showed a smaller KIE for channel closing compared to that of the WT. Unfortunately, information
217 about D187, which is homologous to *Hs*BR D96 and thought to be involved in the proton transfer
218 with E322, could not be obtained due to the lack of significant photocurrents for D187N. However,
219 considering the proton transfer mechanism proposed in the previous study for *Gt*CCR2, where
220 protonation of the cytoplasmic D in TM3 controls channel closing, we hypothesized that a similar
221 mechanism might occur in HulaCCR and the proton transfer from E322 to D187 governs the
222 channel closing there as well.
223
224 **Long N/C-terminal extension of HulaCCR**
225 One of the prominent structural features of HulaCCR is the long N-terminal extension. A careful
226 comparison of HulaCCR to other BCCRs, revealed that the first 12 residues of the expressed
227 construct might not belong to the ORF, which still leaves 79 residues before the first helix of the
228 rhodopsin domain, which exceeds the length of this region in any other BCCRs. The N-terminus
229 harbors a distinctive amino acid sequence, which is predicted as signal peptides by signal peptide
230 prediction methods. The exact cleavage site varied depending on the software used: SignalP 6.0
231 [40] predicted it to be between residues 43 and 44, while TOPCONS[41] predicted the cleavage
232 site between 30 and 31. Similar signal peptides were found in other members of the mgCCR1–3
233 clade. To investigate the role of the N-terminal extension in HulaCCR, two truncated variants were
234 constructed: variant I without the predicted signal sequence region (residues 41–428) and variant
235 II lacking most of the N-terminal region (residues 72–428).
236 No stop codon was observed in the 1285-nt contig encoding HulaCCR, yet the 108 residues
237 of the C-terminal extension were available for analysis. Similarly to other BCCRs, no homology
238 could be detected to known functional domains in the C-terminal extension of HulaCCR, but the
239 structure modeled using AlphaFold2 exhibited two additional helices (Fig. 4a). Based on the

240 structural model, two C-terminal truncations: variants III and IV, were produced by truncating
241 immediately after the predicted TM7 helix (residues 1–341) and after the additional predicted
242 helices after TM7 (residues 1–372), respectively. Patch-clamp measurements were conducted for
243 these four truncated variants (I–IV).

244 Based on the fluorescence images (Fig. 4b), truncated variant I (residues 41–428) exhibited
245 significantly decreased plasma membrane trafficking in cells. When cells showing strong
246 fluorescence were used, no significant photocurrent was obtained. However, significant
247 photocurrents were observed with cells showing relatively lower fluorescence intensity, indicating
248 that mild protein expression improves membrane trafficking of the protein (Fig. 4c). The shape of
249 photocurrents of the truncated variant I did not differ from that of the full-length protein. Hence,
250 the N-terminal extension appears to actually function as a signal peptide enhancing the membrane
251 trafficking of HulaCCR. Intriguingly, truncated variant II, which has a further truncated N-terminus
252 (residues 72–428), membrane translocation was restored, showing an expression pattern and
253 photocurrents similar to those of the full-length protein. We conclude that the region 41–71 between
254 the predicted secretion signal and the rhodopsin domain appears to reduce the localization in the
255 plasma membrane. However, the decreased membrane localization is compensated by the secretion
256 signal peptide (residues 1–41) in the full-length protein. The region spanning the residues 41–71 is
257 predicted by AlphaFold2 to have a disordered structure and is not conserved even among mgCCR1-
258 like ChRs.

259 For the C-terminal truncated variants, truncated variant III, which is composed of the residues
260 1–341 and truncated immediately after TM7, showed an increase in fluorescence intensity inside
261 the cells (Fig. 4b), indicating a decreased membrane localization compared to that of the full-length
262 HulaCCR. Truncated variant IV, in which a predicted disordered region beyond an additional
263 cytoplasmic helix was removed, exhibited higher membrane localization than that of truncated

variant III. The photocurrents of truncated variants III and IV were similar to that of the full-length HulaCCR, indicating that the C-terminal extended region is not as essential as the N-terminal one (Fig. 4c).

HulaCCR is able to drive neuronal firing

Our findings suggest that HulaCCR exhibits cation conductance and ion selectivity similar to those of *Gt*CCR4 and ChRmine, indicating its potential as an optogenetic tool to induce neuronal firing using light as other CCRs. To assess the practical utility of HulaCCR as an optogenetic tool, primary cultures of rat hippocampal neurons were transfected with HulaCCR, and its expression was confirmed based on the fluorescence signal (Fig. 5a). HulaCCR was well expressed throughout the neuronal cells, including the axon. Patch-clamp recordings were performed on neurons expressing HulaCCR (Fig. 5b), and upon 200 ms light stimulation, neuronal firings were elicited. Additionally, even with 5 ms light stimulation at 10 Hz, continuous neuronal firing was observed, demonstrating HulaCCR's ability to control neuronal activity through light stimulation. This is likely facilitated by the relatively high conductance of HulaCCR to sodium.

Discussion

In this study, HulaCCR was identified as a new CCR featuring the ETD motif. Considering cation selectivity, P_{Na+}/P_{H+} was previously estimated for *Cr*ChR2 and several other CCRs. While HulaCCR exhibits a P_{Na+}/P_{H+} value of $(1.5 \pm 0.1) \times 10^{-5}$, P_{Na+}/P_{H+} of *Cr*ChR2 is approximately 1×10^{-6}.[8] *Gt*CCR4, with a value of about 5×10^{-5}, has been reported as a CCR with low proton selectivity,[27] suggesting that HulaCCR also has relatively low proton selectivity like *Gt*CCR4 among CCRs. The P_{X+}/P_{H+} values obtained for HulaCCR do not differ significantly between the different alkali-metal monovalent cations, indicating similar permeability levels for all of them.

288 The photocurrents derived from Cs^+ in HulaCCR do not significantly differ from that of Na^+,
289 whereas the photocurrents from Cs^+ are approximately half of that from Na^+ in *Gt*CCR4.[27] Hence,
290 HulaCCR likely possesses a relatively large channel pore facilitating the transport of large
291 monovalent cations. This is further supported by the fact Li^+, which is strongly hydrated in
292 solution,[42] showed permeability comparable to other monovalent cations. Considering the
293 expected large pore size capable of efficient Cs^+ transport, it is likely that partially hydrated Li^+ is
294 stabilized within the pore rather than undergoing complete dehydration. mgCCR1[23] despite
295 sharing the ETD motif with HulaCCR and having a 48% amino acid sequence identity, exhibits
296 relatively high proton selectivity compared to HulaCCR. The significant difference in ion
297 selectivity despite the relatively high amino acid sequence identity is intriguing. A comparison of
298 predicted structures using AlphaFold2 and cavities potentially involved in channel gating did not
299 suggest significant differences in the size of channel pore (Fig. S4). Hence, although it is anticipated
300 that the structural changes in the open state of HulaCCR are larger than that in mgCCR1, leading
301 an opening of a larger channel that is capable of conducting large monovalent cations, further
302 investigation is needed to clarify the reason of different cation selectivity between HulaCCR and
303 mgCCR1.

304 Considering the role of the first motif residue E, it was found to influence the absorption
305 spectrum and gating (Figs. 3b–d). In the E176D mutant, the time constants of channel opening and
306 closing were altered compared to the WT, and regarding the fast channel closing component, the
307 closing time constant was 1.8 and 1.3 times slower than that of the wild type at a +40 mV and a
308 −60 mV membrane potential, respectively, indicating the difference in the closing rate between
309 HulaCCR E176D and the WT becomes larger at positive membrane potential. Hence, in the WT,
310 E187 appears to enhance inward rectification. Indeed, when observing the photocurrent upon 200
311 ms illumination, the positive photocurrent intensity in the WT is slightly suppressed compared to

312 E176D (Figure S2d). This suggests that the glutamate is one of the important residues defining the
313 rectification properties of HulaCCR.

314 Looking at the photocurrents of the C303A mutant involving the residue immediately before
315 the retinal-binding lysine residue in TM7 at 200 ms light illumination, we find that the decay rate
316 after light off is significantly slower compared to that of the WT (WT = 17 ± 2 ms, C303A = 130
317 ± 20 ms, at −60 mV, n = 5) (Fig. S2d). *Gt*ACR1, a member of the cryptophyte ACR family, also
318 has a cysteine at this position, C237, and an analogous mutation, C237A, was reported to eliminate
319 one of the two closing components and to show approximately 1.8 times slower closing rate for the
320 remaining component.[43] However, the retardation effect of the corresponding mutation on the
321 closing rate is much higher in HulaCCR (7.6 times slower), indicating that C303 is likely to
322 influence the closing rate through a mechanism different from that of *Gt*ACR1. Since C303 is
323 located close to the retinal Schiff base, the mutation of this residue may affect the photochemical
324 reactions around the chromophore. Nevertheless, we observed no significant spectral shift between
325 HulaCCR C303A and the WT based on the action spectra of the photocurrent, contrasting with the
326 red shift in C237A of *Gt*ACR1[43] (Fig. S2c). Hence, the interaction between the retinal
327 chromophore and C303 in HulaCCR is different from that in *Gt*ACR1, and the effect on the closing
328 process differs even with the identical mutation.

329 The N-terminal extension, outside the seven TM helices constituting the rhodopsin domain,
330 contains a sequence predicted as a secretion signal sequence, and our results suggest that this
331 secretion signal sequence rescues the decrease in membrane translocation caused by the sequence
332 between residues 41 and 71. mgCCR1 has a similarly long N-terminal extension, although it is
333 shorter and demonstrates low homology to that of HulaCCR. Analogously, the N-terminal
334 extension of mgCCR1 is predicted to have signal peptide cleaved between positions 24 and 25
335 (according to SignalP 6.0). Hence, it is anticipated that a similar mechanism maintains protein

membrane translocation in mgCCR1 as well. Regarding the extension at the C-terminus, although not as prominent as the N-terminus, a slight decrease in membrane translocation compared to the full-length protein was observed in variant III (residues 1–341) (Fig. 4b). Hence, the C-terminal region may contribute to maintaining the stability of proteins in the membrane by interacting with the cytoplasmic surface of the rhodopsin part. The long C-terminal extensions of green algal CCRs, prasinophyte ACRs and labyrinthulean ACRs have been found to contain response regulator-like domains[44] as well as additional conserved domains of unknown function,[44,45] but we could not identify any such functional domains in HulaCCR or other BCCRs. It has been previously reported that multiple arginines within the C-terminal extension interact with the rhodopsin part and regulate the closing rate.[46] HulaCCR also has several arginines between residues 352 and 358 that were truncated in variant III. Moreover, a slightly slower decay rate after light off was observed in variant III compared to that of the WT upon 200 ms light illumination (WT = 17 ± 2 ms, variant III = 21 ± 1 ms, at −60 mV, n = 5), exhibiting behavior similar to *Kn*ChR. Hence, it is conceivable that in structural stabilization in the membrane is facilitated by electrostatic interactions between the C-terminal extension and the cytoplasmic side of the rhodopsin domain mediated by the arginines, potentially influencing gating kinetics.

352 **Figures**

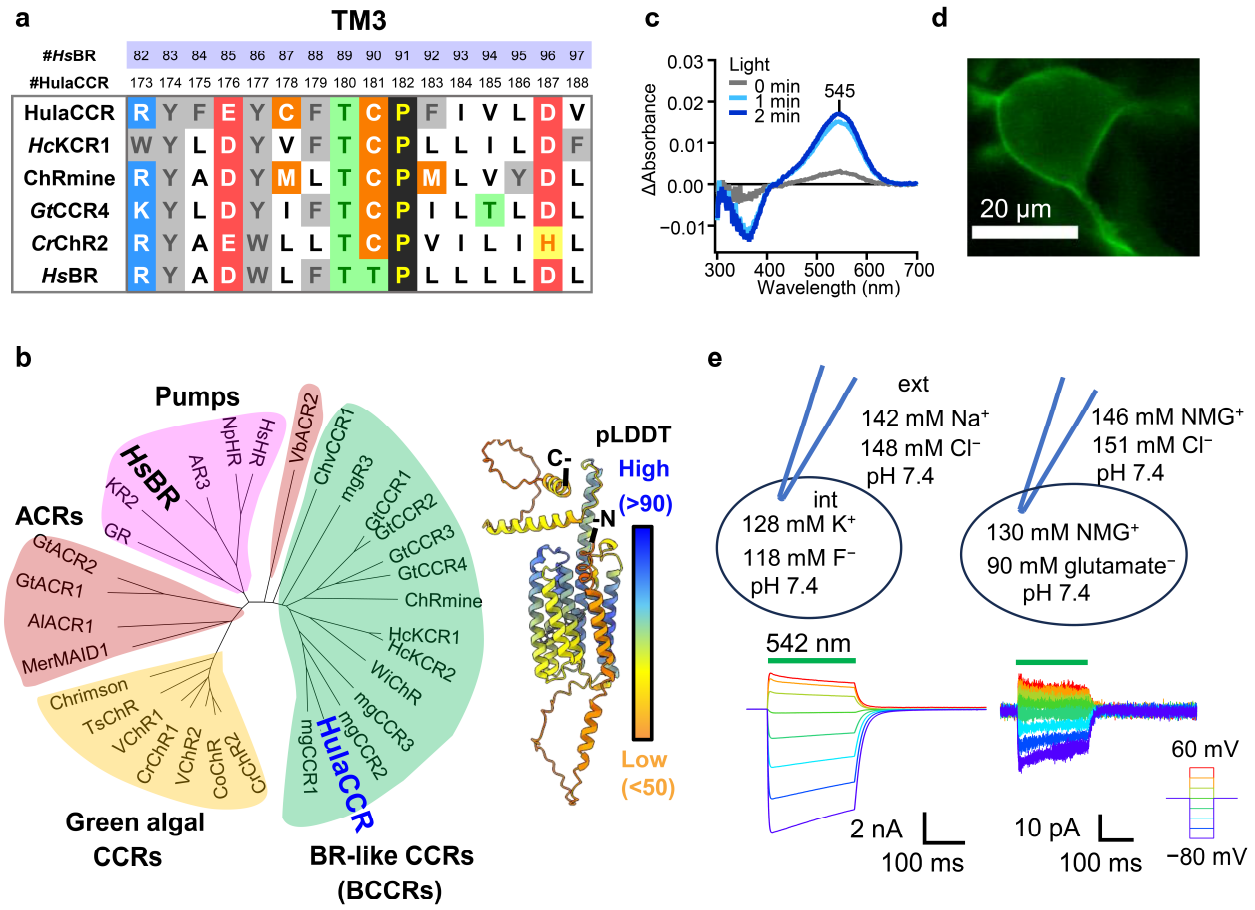

353

354 **Fig. 1. Characterization of HulaCCR**

355 **a** Amino acid alignment of TM3 of HulaCCR with *Hc*KCR1, ChRmine, *Gt*CCR4, *Cr*ChR2, and
356 *Hs*BR. **b** (left) The phylogenetic tree of known ion-pumping rhodopsins, channelrhodopsins, and
357 HulaCCR. The phylogenetic tree was inferred using the neighbor-joining method of MEGA X
358 software (version 11.0.13). (right) Schematic illustration of HulaCCR structure based on
359 AlphaFold2 prediction. **c** Difference UV–visible absorption spectra showing the λ_{max} of HulaCCR.
360 The difference spectra were measured upon the hydrolysis reaction of the retinal Schiff-base
361 linkage induced by hydroxylamine with visible light illumination (0, 1, or 2 min). **d** Fluorescent
362 image of ND7/23 cells expressing HulaCCR which is C-terminally labeled with EYFP (Scale bar
363 = 20 μm). **e** Photocurrents of HulaCCR at 142 mM $[Na^+]_{out}$ and 128 mM $[K^+]_{in}$ at pH = 7.4 (left)

364 and at 146 mM $[NMG^+]_{out}$ and 130 mM $[NMG^+]_{in}$ at pH = 7.4 (right).

365

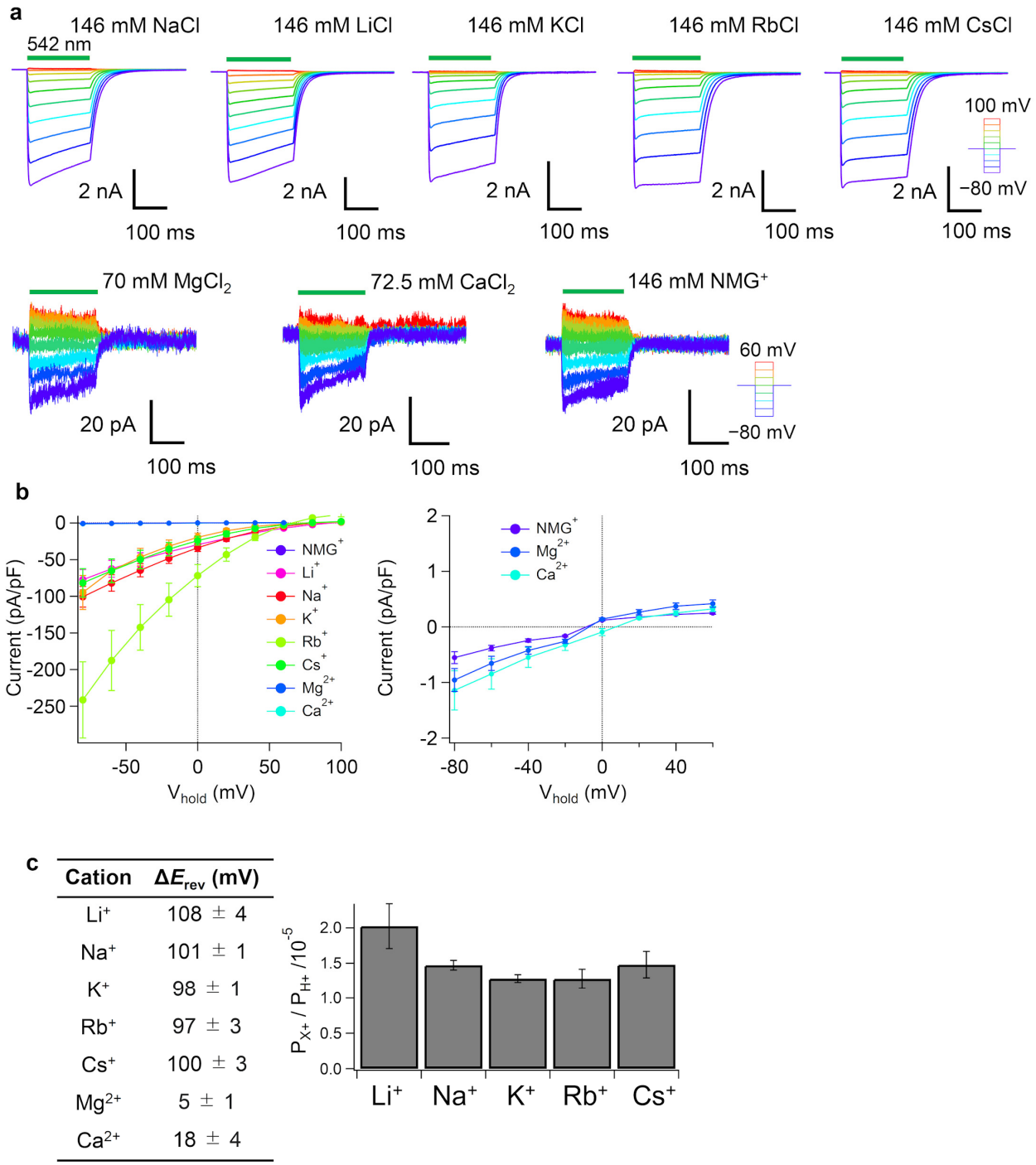

Cation	ΔE_{rev} (mV)
Li^+	108 ± 4
Na^+	101 ± 1
K^+	98 ± 1
Rb^+	97 ± 3
Cs^+	100 ± 3
Mg^{2+}	5 ± 1
Ca^{2+}	18 ± 4

366

367 **Fig. 2. Ion selectivity of HulaCCR**

368 **a** Representative photocurrent traces of HulaCCR at 146 mM $[X^+]_{out}$ and 130 mM $[NMG^+]_{in}$ (top),

369 and at 70 mM $[Mg^{2+}]_{out}$ /72.5 mM $[Ca^{2+}]_{out}$ /146 mM $[NMG^+]_{out}$ and 130 mM $[NMG^+]_{in}$ (bottom).

370 **b** The *I*–*V* plot of HulaCCR photocurrents with different extracellular cations (mean ± S.E., $n = 6$).

371 **d** Difference in E_{rev} between different cations and H^+ (ΔE_{rev}) (left) and relative permeability of

372 different cations against H^+ (P_{X+}/P_{H+}) (right) (mean ± S.E., $n = 6$).

373

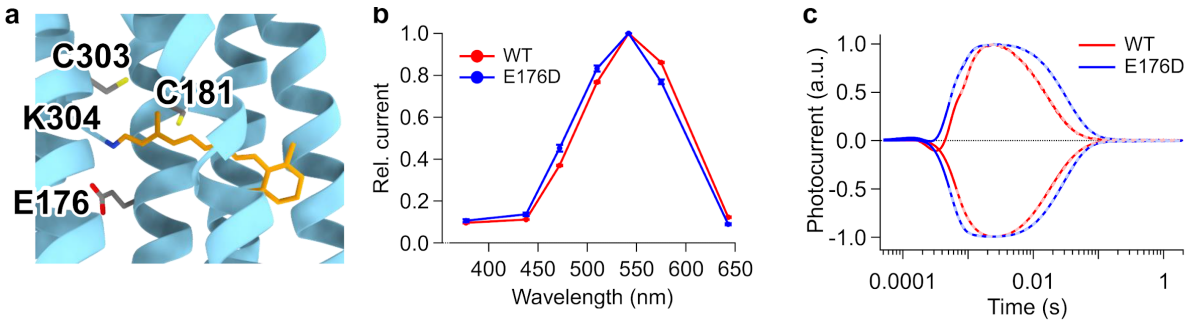

d

	$Open_{fast}$ /ms (contribution)	$Open_{slow}$ /ms (contribution)	$Close_{fast}$ /ms (contribution)	$Close_{slow}$ /ms (contribution)
WT 40mV	0.40 ± 0.01 (93.6 ± 0.4%)	3.6 ± 0.2 (6.4 ± 0.4%)	14.6 ± 0.1 (96.0 ± 0.4%)	42 ± 2 (4.0 ± 0.4%)
E176D 40 mV	0.33 ± 0.01 (89.7 ± 0.5%)	7.3 ± 0.3 (10.3 ± 0.5%)	26.8 ± 0.1 (99.2 ± 0.1%)	300 ± 40 (0.8 ± 0.1%)
WT −60mV	0.34 ± 0.01 (87 ± 1%)	4.4 ± 0.4 (13 ± 1%)	15.8 ± 0.5 (87±1%)	47 ± 2 (13±1%)
E176D −60 mV	0.26 ± 0.01 (87.5 ± 0.5%)	8.4 ± 0.4 (12.5 ± 0.5%)	20.4 ± 0.1 (99.5 ± 0.1%)	200 ± 20 (0.5 ± 0.1%)

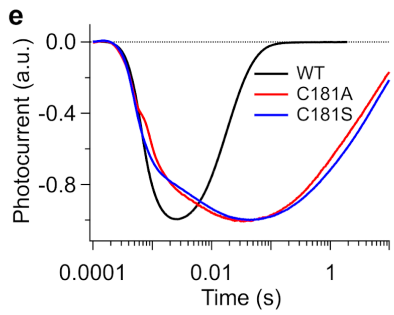

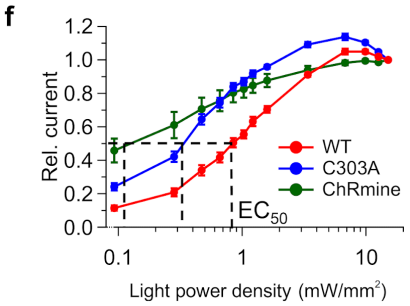

374

375 **Fig. 3. Effect of point mutation**

376 **a** AlphaFold2 structural model for HulaCCR showing the mutated residues. The retinal structure

377 (orange) and the side chain of conjugated lysine are of *Hc*KCR1 (PDB ID: 8H86). **b** Normalized

378 action spectra of the HulaCCR WT and E176D (mean ± S.E., $n = 5$). **c** Photocurrent traces of the

379 WT and E176D upon nanosecond laser flash excitation at holding potentials of 40 mV (positive)

380 and −60 mV (negative). Photocurrents were recorded at 133 mM $[Na^+]_{out}$ and 120 mM $[Na^+]_{in}$ at

pH = 7.4. Fitting curves are shown as broken lines. **d** Time constants of channel opening and closing of the WT HulaCCR and E176D (mean ± S.E., n = 9). **e** Photocurrent traces of the HulaCCR WT, C181A, and C181S upon nanosecond laser flash excitation recorded with standard pipette and extracellular solutions. **f** Light-power dependency of the photocurrent of HulaCCR WT, C303A, and ChRmine at −40 mV with standard pipette and extracellular solutions (mean ± S.E., n = 5).

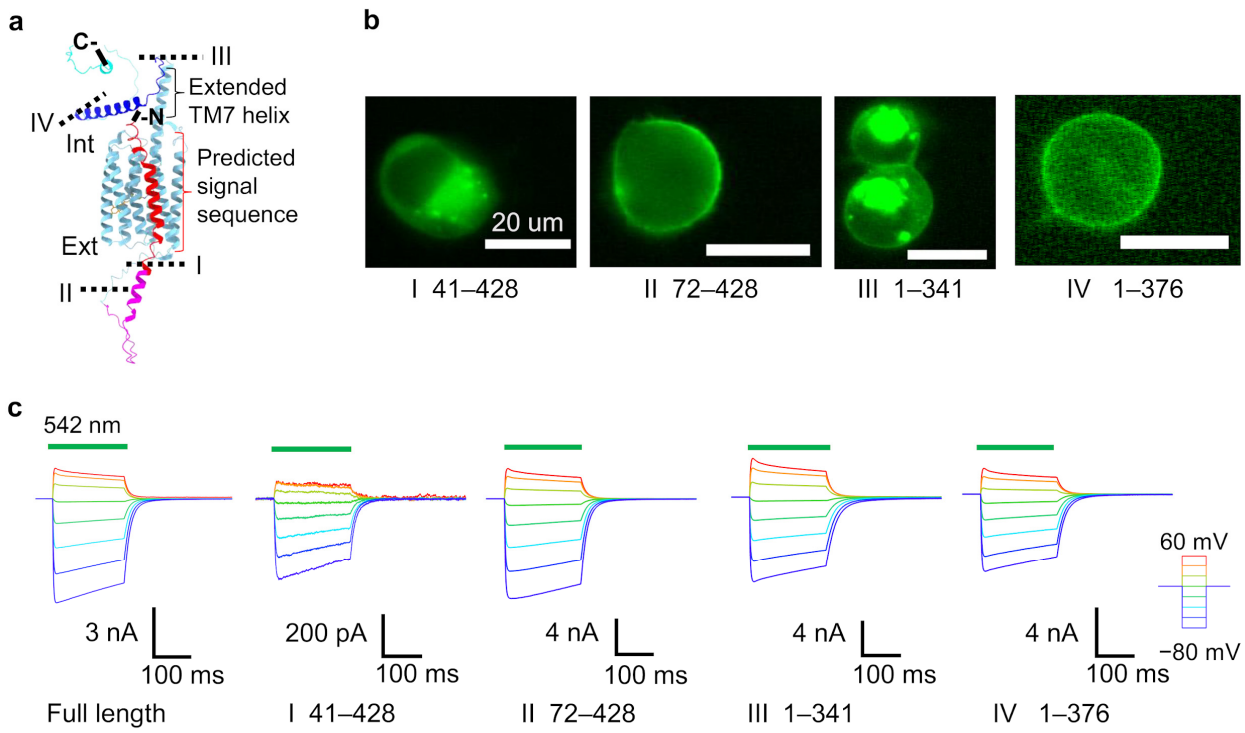

Fig. 4. Long N/C-terminal extensions of HulaCCR

a Truncated sites shown in the AlphaFold2 structural model of HulaCCR. **b** Fluorescent images of truncated variants expressed in ND7/23 cells. Scale bars, 20 µm. **c** Representative photocurrent traces of truncated variants recorded with standard pipette and extracellular solutions.

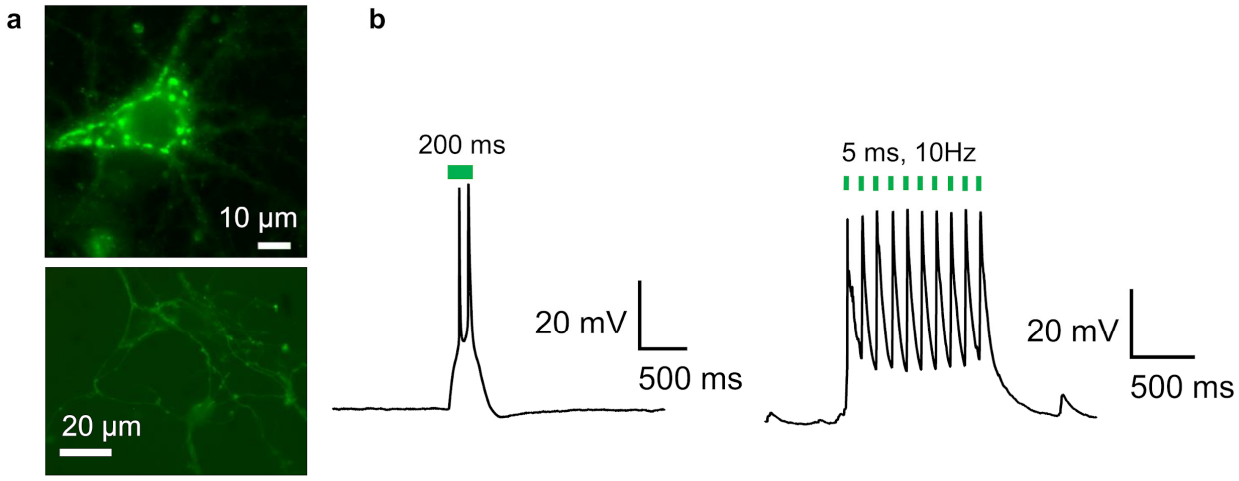

Fig. 5. Light stimulation of hippocampal neurons expressing HulaCCR

a Fluorescent images of cell body (top) and axon (bottom) of a hippocampal neuron expressing HulaCCR. **b** Voltage traces showing depolarization and spikes of the neuron in response to 200 ms green (542 nm) light stimulation (left) and to 10 Hz stimulation with 5 ms pulses (right).

398 **Materials and Methods**

399

400 **Sampling, RNA extraction, and Rhodopsin screening**

401 Peat lake sampling was performed on February 23rd, 2021 in The Hula Nature Reserve, Israel (33°04'33.8"N
402 35°36'40.8"E). 20 L of water from the surface and 0.5 m depth was filtered through a 50 µm mesh net to
403 remove large particles, filtered onto a GF/D filter (Whatman), and flash-frozen using liquid nitrogen on-site.
404 Total RNA was extracted from frozen filters, corresponding to ~5 L per sample (RNeasy PowerSoil
405 Total RNA Kit; Qiagen). The RNA was tested with Bioanalyzer, and PolyA-selected libraries were
406 constructed and sequenced at the Weizmann Institute of Science, on the NovaSeq platform (300 cycles, PE).
407 *De-Novo* assembly was done post trimming (Trimgalore; v. 0.6.6 [DOI 10.5281/zenodo.5127898],
408 Cutadapt; v. 3.4[47] with MEGAHIT (v. 1.2.9)[48] and then clustered for redundancy (cd-hit-est; v. 4.8.1)
409 [49]. Rhodopsin screening was done with HMMsearch (v. 3.3.2)[50] with the microbial rhodopsin profiles
410 from https://github.com/BejaLab/RhodopsinProfiles.

411

412 **DNA constructs**

413 Coding sequence (Table S1) of full-length HulaCCR was cloned into pCMV3.0-enhanced
414 fluorescent yellow protein (EYFP) vector between EcoRI and BamHI sites with a Kir2.1 membrane
415 trafficking signal, EYFP, and an ER-export signal[51] fused at the C-terminus of HulaCCR. For
416 point mutations, the QuikChange site-directed mutagenesis method (Agilent Technologies, CA)
417 was employed according to a manufacturer standard protocol. The truncated mutants were PCR-
418 based cloned using EcoRI-BamHI restriction sites into the pCMV3.0-EYFP vector. Primers used
419 in DNA work are listed in Table S2.

420

421 **UV–visible spectroscopy**

422 Cell culture and transfection for UV–visible spectroscopy were conducted as described

423 elsewhere.[52] Briefly, COS-1 cells (cell number: JCRB9082; Japanese Collection of Research
424 Bioresources Cell Bank, Osaka, Japan) were transfected by the polyethyleneimine method.[53]
425 Cells were supplemented with 2.5 μM all-*trans*-retinal (ATR) on the following day and harvested
426 after 48 h of transfection. The cell membranes were solubilized with a phosphate buffer (pH 7.0)
427 containing (in mM) 66.5 phosphate, 133 NaCl with 3% *n*-dodecyl-β-D-maltoside. After
428 centrifugation (21,600 × g, 20°C, 5 min), the supernatant was subjected for the measurement of
429 UV–visible absorption spectra using a spectrophotometer (V-730, JASCO, Japan). Rhodopsin was
430 bleached by hydroxylamine (50 mM) and illumination with visible light from a 1-kW Xe lamp
431 (MAX-303, Asahi Spectra, Japan) through a long-pass filter (Y52, AGC Techno Glass, Japan).
432 Difference spectra were calculated by subtracting post-illumination spectra from the pre-
433 illumination spectrum. To correct for spectral changes derived from non-rhodopsin components in
434 the sample, the corresponding spectra of untransfected cell membranes that underwent the same
435 treatment as the sample were subtracted from the sample spectra.
436
437
438 **Cell culture and transfection for electrophysiology**
439 ND7/23 cells were grown in Dulbecco's modified Eagle's medium (D-MEM, FUJIFILM Wako
440 Pure Chemical Co., Japan) supplemented with 5% fetal bovine serum (FBS) under a 5% CO_2
441 atmosphere at 37°C. ND7/23 cells were attached onto a collagen-coated 12-mm coverslips (IWAKI,
442 cat. 4912-010, Japan) placing in a 4-well cell culture plate (SPL Life Sciences, cat. 30004, Korea).
443 The expression plasmids were transiently transfected in ND7/23 cells using Lipofectamine 3000
444 transfection reagent (Thermo Fisher Scientific Inc., MA). Seven to eight hours after the transfection,
445 the medium was replaced with D-MEM containing 10% horse serum (New Zealand origin, Thermo
446 Fisher Scientific Inc., MA), 50 ng mL^{-1} nerve growth factor-7S (Sigma-Aldrich, MO), 1 mM N^6,2'-

447 O-dibutyryladenosine-3',5'-cyclic monophosphate sodium salt (Nacalai tesque, Japan), 1 μM
448 cytosine-1-β-D(+)-arabinofuranoside (FUJIFILM Wako Pure Chemical Co., Japan), and 2.5 μM
449 all-*trans*-retinal. Electrophysiological recordings were conducted at 1–3 days after the transfection.
450 The transfected cells were identified by observing the EYFP fluorescence under an up-right
451 microscope (BX50WI, Olympus, Japan).

452 Hippocampi were isolated from postnatal day 1 (P1) Wistar-ST rats (by Sankyo Labo
453 Service Co., Japan) and treated with papain dissociation system (Worthington Biochemical Co.,
454 NJ) according to the company protocol. Briefly, dissected hippocampi were treated with papain for
455 1 h at 37°C. The dissociated cells were washed with Earle's Balanced Salt Solution (EBSS)
456 supplemented with ovomucoid protease inhibitor with bovine serum albumin. The dissociated cells
457 were resuspended in culture medium (Neurobasal A containing 2% B-27 plus (Thermo Fisher
458 Scientific Inc., MA)). Approximately 150,000 cells were plated on 12-mm poly-L-lysine-coated
459 glass coverslips (IWAKI, cat. 4912-040, Japan) in the 4-well cell culture plate. Transfection was
460 done by adeno-associated virus (AAV), and the plasmid and virus packaging were synthesized by
461 Vectorbuilder Inc. The plasmid pAAV vector has a CaMKIIa promotor containing the sequence of
462 HulaCCR, C-terminally fused to the Kir2.1 membrane trafficking signal followed by EYFP and
463 the ER export signal. For transfection, AAV8 was added to each well (4–8 × 10^8 genome copies
464 $well^{-1}$) 7 days after plating. The electrophysiological recordings were performed 15–22 days after
465 transfection.

466

467 **Electrophysiology**

468 All experiments were carried out at room temperature (20–22°C). Currents were recorded using an
469 EPC-8 amplifier (HEKA Electronic, Germany) under a whole-cell patch clamp configuration. The
470 data were filtered at 1 kHz, sampled at 50 kHz (Digidata1440 A/D, Molecular Devices Co., CA)

471 and stored in a computer (pClamp11.1, Molecular Devices). The standard internal pipette solutions
472 for the whole-cell voltage clamp recordings from the ND7/23 cells contained (in mM) 119 KF, 10
473 KOH, 5 Na_2EGTA, 14 HEPES, 0.0025 ATR (pH 7.4 adjusted with HCl). The standard extracellular
474 solution contained (in mM): 138 NaCl, 3 KCl, 2.5 $CaCl_2$, 1 $MgCl_2$, 10 HEPES, 4 NaOH, and 11
475 glucose (pH 7.4 adjusted with HCl). In the ion selectivity measurement, extracellular solution
476 contained (in mM) 146 XCl (X = Na^+, K^+, Li^+, Rb^+, Cs^+), 6 N methyl-D-glucamine (NMG), 2.5
477 $CaCl_2$, 10 HEPES, 11 glucose (pH 7.4 adjusted with HCl). For the divalent cation selectivity,
478 extracellular solution contained (in mM) 70 XCl_2 (X = Ca^{2+}, Mg^{2+}), 6 NMG, 2.5 $CaCl_2$, 10 HEPES,
479 11 glucose (pH 7.4 adjusted with HCl). The NMG-extracellular solution contained (mM) 146 NMG,
480 146 HCl, 2.5 $CaCl_2$, 10 HEPES, and 11 glucose (pH 7.4 adjusted with NMG). The NMG-pipette
481 solution contained (in mM) 130 NMG, 90 glutamate, 6 $(NMG)_2EGTA$, 50 HEPES, 2.5 $MgSO_4$, 2.5
482 MgATP, 0.0025 ATR (pH 7.4 adjusted with H_2SO_4). The liquid junction potentials (LJPs) were
483 calculated by pClamp 11.1 software (Table. S3) and estimated reversal potentials were
484 compensated by calculated LJPs.

485 For whole-cell voltage clamp, illumination at 377 ± 25, 438 ± 12, 472 ± 15, 510 ± 5, 542
486 ± 13, 575 ± 12 or 643 ± 10 nm was carried out using a SpectraX light engine (Lumencor Inc., OR)
487 controlled by pClamp 11.1 software. HulaCCR was illuminated through an objective lens
488 (LUMPlan FL 40x, NA 0.80W, Olympus, Japan). For the standard photocurrent detection, the
489 power of the 542-nm light was directly measured under a microscope using a visible light-sensing
490 thermopile (MIR178 101Q, SSC Co., Ltd., Japan) and was adjusted to 13.3 mW mm^{-2}. The action
491 spectrum was measured at a holding potential of −40 mV at wavelengths with equivalent power
492 density of 0.8 mW mm^{-2}. Each action spectrum was estimated by the maximal amplitude of the
493 photocurrent scaled by the light power density under the assumption of a linear relationship
494 between the photocurrent intensity and the light power density.

For Laser-flash patch clamp experiment, a laser flash (3–5 ns) at 532 nm (Nd:YAG laser, Minilite II, Continuum, CA) was used.[39] For measuring the KIE on the gating dynamics, the internal pipette solutions were made of H_2O or D_2O solutions containing (in mM) 60 Na_2SO_4, 25 NMG, 60 mannitol, 5 EGTA, 10 HEPES, 2.5 $MgSO_4$, 2.5 MgATP, and 0.0025 ATR adjusting pH to 7.4 with HCl or DCl, respectively. The extracellular solutions were made of H_2O or D_2O solutions containing (in mM) 133 NaCl, 3 KCl, 5 NMG, 10 HEPES, 5 $CaCO_3$ (solved by HCl or DCl solutions), 2.5 $MgSO_4$ and 11 glucose, adjusting pH to 7.4 with HCl or DCl, respectively. The pipette resistance was adjusted to 3–5 MΩ with a series resistance of 7–19 MΩ (WT; 12 ± 1, n = 9 for H_2O; 16 ± 1, n = 9 for D_2O, E176D; 9 ± 1, n = 9 for H_2O, E322Q; 10 ± 1, n = 9 for H_2O; 15 ± 1, n = 9 for D_2O) and a cell capacitance of 30–90 pF (WT; 63 ± 4, n = 9 for H_2O; 58 ± 3, n = 9 for D_2O, E176D; 50 ± 2, n = 9 for H_2O, E322Q; 43 ± 3, n = 9 for H_2O; 44 ± 2, n = 9 for D_2O). In every experiment, the series resistance was compensated for by 70%. Obtained signals had electrical noise from the laser system. Therefore, the noise signal recorded without light excitation was subtracted from raw photocurrent traces.

For whole-cell recordings in cultured hippocampal neurons, patch pipettes were filled with (in mM) 90 potassium gluconate, 30 KOH, 49 HEPES, 2.5 $MgCl_2$, 2.5 MgATP, 5 Na_2EGTA, and 0.0025 ATR, titrated to pH 7.4. The extracellular solution contained (in mM) 138 NaCl, 3 KCl, 2.5 $CaCl_2$, 1 $MgCl_2$, 11 glucose, and 10 HEPES, 2 kynurenic acid, titrated to pH 7.4.

Acknowledgements

We thank Ariel Chazan, Shirley Larom, David Iluz, Said Abu-Ghosh, and the park rangers David Zaguri and Ido Shaked for help in sampling, and the Israel Nature and Parks Authority for the permit to sample in The Hula Nature Reserve. This work was supported by JSPS KAKENHI Grants-in-Aid (grant JP 23K14151 to S.T., JP 21H01875, JP23K18090, and JP23H04404 to K.I.),

JST CERST (grant JPMJCR22N2 to K.I.), and MEXT Promotion of Development of a Joint Usage/ Research System Project: Coalition of Universities for Research Excellence Program (CURE) (grant JPMXP1323015482 to K.I.), the European Commission, under Horizon Europe's research and innovation programme (Bluetools project, Grant Agreement No 101081957 to O.B.), the Israel Science Foundation (Research Center grant 3131/20 to O.B.), and the Nancy and Stephen Grand Technion Energy Program (GTEP). O.B. holds the Louis and Lyra Richmond Chair in Life Sciences.

References

[1] A. Rozenberg, K. Inoue, H. Kandori, O. Béjà, Microbial rhodopsins: The last two decades, Annu. Rev. Microbiol. 75 (2021) 427–447.

[2] O.P. Ernst, D.T. Lodowski, M. Elstner, P. Hegemann, L.S. Brown, H. Kandori, Microbial and animal rhodopsins: structures, functions, and molecular mechanisms, Chem. Rev. 114 (2014) 126–163.

[3] T. Nagata, K. Inoue, Rhodopsins at a glance, J. Cell Sci. 134 (2021) jcs258989.

[4] K. Deisseroth, P. Hegemann, The form and function of channelrhodopsin, Science 357 (2017) eaan5544.

[5] V. Emiliani, E. Entcheva, R. Hedrich, P. Hegemann, K.R. Konrad, C. Lüscher, M. Mahn, Z.-H. Pan, R.R. Sims, J. Vierock, O. Yizhar, Optogenetics for light control of biological systems, Nat. Rev. Methods Primers 2 (2022) 55.

[6] O.A. Sineshchekov, K.-H. Jung, J.L. Spudich, Two rhodopsins mediate phototaxis to low- and high-intensity light in *Chlamydomonas reinhardtii*, Proc. Natl. Acad. Sci. U. S. A. 99 (2002) 8689–8694.

[7] G. Nagel, D. Ollig, M. Fuhrmann, S. Kateriya, A.M. Musti, E. Bamberg, P. Hegemann, Channelrhodopsin-1: a light-gated proton channel in green algae, Science 296 (2002) 2395–2398.

[8] G. Nagel, T. Szellas, W. Huhn, S. Kateriya, N. Adeishvili, P. Berthold, D. Ollig, P. Hegemann, E. Bamberg, Channelrhodopsin-2, a directly light-gated cation-selective membrane channel, Proc. Natl. Acad. Sci. U. S. A. 100 (2003) 13940–13945.

[9] E.G. Govorunova, O.A. Sineshchekov, R. Janz, X. Liu, J.L. Spudich, Natural light-gated anion channels: A family of microbial rhodopsins for advanced optogenetics, Science 349 (2015) 647–650.

[10] E.G. Govorunova, O.A. Sineshchekov, J.L. Spudich, Structurally distinct cation channelrhodopsins from cryptophyte algae, Biophys. J. 110 (2016) 2302–2304.

[11] H. Hagio, W. Koyama, S. Hosaka, A.D. Song, J. Narantsatsral, K. Matsuda, T. Shimizu, S. Hososhima, S.P. Tsunoda, H. Kandori, M. Hibi, Optogenetic manipulation of neuronal and cardiomyocyte functions in zebrafish using microbial rhodopsins and adenylyl cyclases, eLife 12 (2023) e83975.

[12] M. Mahn, L. Gibor, P. Patil, K. Cohen-Kashi Malina, S. Oring, Y. Printz, R. Levy, I. Lampl, O. Yizhar, High-efficiency optogenetic silencing with soma-targeted anion-conducting channelrhodopsins, Nat. Commun. 9 (2018) 4125.

[13] S. Huang, M. Ding, M.R.G. Roelfsema, I. Dreyer, S. Scherzer, K.A.S. Al-Rasheid, S. Gao, G. Nagel, R. Hedrich, K.R. Konrad, Optogenetic control of the guard cell membrane potential and stomatal movement by the light-gated anion channel *Gt*ACR1, Sci. Adv. 7 (2021) eabg4619.

[14] Y. Zhou, M. Ding, S. Gao, J. Yu-Strzelczyk, M. Krischke, X. Duan, J. Leide, M. Riederer, M.J. Mueller, R. Hedrich, K.R. Konrad, G. Nagel, Optogenetic control of plant growth by a microbial rhodopsin, Nat. Plants 7 (2021) 144–151.

[15] H. Kandori, Ion-pumping microbial rhodopsins, Front. Mol. Biosci. 2 (2015) 52.

[16] E.G. Govorunova, O.A. Sineshchekov, J.L. Spudich, Structurally distinct cation channelrhodopsins from cryptophyte algae, Biophys. J. 110 (2016) 2302–2304.

[17] Y. Yamauchi, M. Konno, S. Ito, S.P. Tsunoda, K. Inoue, H. Kandori, Molecular properties of a DTD channelrhodopsin from *Guillardia theta*, Biophys Physicobiol. 14 (2017) 57–66.

[18] J.H. Marshel, Y.S. Kim, T.A. Machado, S. Quirin, B. Benson, J. Kadmon, C. Raja, A. Chibukhchyan, C. Ramakrishnan, M. Inoue, J.C. Shane, D.J. McKnight, S. Yoshizawa, H.E.

Kato, S. Ganguli, K. Deisseroth, Cortical layer-specific critical dynamics triggering perception, Science 365 (2019) eaaw5202.
[19] R. Chen, F. Gore, Q.-A. Nguyen, C. Ramakrishnan, S. Patel, S.H. Kim, M. Raffiee, Y.S. Kim, B. Hsueh, E. Krook-Magnusson, I. Soltesz, K. Deisseroth, Deep brain optogenetics without intracranial surgery, Nat. Biotechnol. 39 (2021) 161–164.
[20] H.E. Kato, Structure–Function Relationship of Channelrhodopsins, in: H. Yawo, H. Kandori, A. Koizumi, R. Kageyama (Eds.), Optogenetics: Light-sensing proteins and their applications in neuroscience and beyond, Springer Singapore, Singapore, 2021: pp. 35–53.
[21] E.G. Govorunova, Y. Gou, O.A. Sineshchekov, H. Li, X. Lu, Y. Wang, L.S. Brown, F. St-Pierre, M. Xue, J.L. Spudich, Kalium channelrhodopsins are natural light-gated potassium channels that mediate optogenetic inhibition, Nat. Neurosci. 25 (2022) 967–974.
[22] J. Vierock, E. Shiewer, C. Grimm, A. Rozenberg, I.-W. Chen, L. Tillert, A.G. Castro Scalise, M. Casini, S. Augustin, D. Tanese, B.C. Forget, R. Peyronnet, F. Schneider-Warme, V. Emiliani, O. Béjà, P. Hegemann, WiChR, a highly potassium-selective channelrhodopsin for low-light one- and two-photon inhibition of excitable cells, Sci. Adv. 8 (2022) eadd7729.
[23] E.G. Govorunova, O.A. Sineshchekov, L.S. Brown, A.-N. Bondar, J.L. Spudich, Structural foundations of potassium selectivity in channelrhodopsins, MBio 13 (2022) e0303922.
[24] M. Mirdita, K. Schütze, Y. Moriwaki, L. Heo, S. Ovchinnikov, M. Steinegger, ColabFold: making protein folding accessible to all, Nat. Methods 19 (2022) 679–682.
[25] K. Inoue, M. Karasuyama, R. Nakamura, M. Konno, D. Yamada, K. Mannen, T. Nagata, Y. Inatsu, H. Yawo, K. Yura, O. Béjà, H. Kandori, I. Takeuchi, Exploration of natural red-shifted rhodopsins using a machine learning-based Bayesian experimental design, Commun. Biol. 4 (2021) 362.
[26] C.A. Lewis, Ion-concentration dependence of the reversal potential and the single channel conductance of ion channels at the frog neuromuscular junction, J. Physiol. 286 (1979) 417–445.
[27] S. Shigemura, S. Hososhima, H. Kandori, S.P. Tsunoda, Ion channel properties of a cation channelrhodopsin, *Gt*_CCR4, Appl. Sci. 9 (2019) 3440.
[28] K.E. Kishi, Y.S. Kim, M. Fukuda, M. Inoue, T. Kusakizako, P.Y. Wang, C. Ramakrishnan, E.F.X. Byrne, E. Thadhani, J.M. Paggi, T.E. Matsui, K. Yamashita, T. Nagata, M. Konno, S. Quirin, M. Lo, T. Benster, T. Uemura, K. Liu, M. Shibata, N. Nomura, S. Iwata, O. Nureki, R.O. Dror, K. Inoue, K. Deisseroth, H.E. Kato, Structural basis for channel conduction in the pump-like channelrhodopsin ChRmine, Cell 185 (2022) 672-689.e23.
[29] M. Nack, I. Radu, M. Gossing, C. Bamann, E. Bamberg, G.F. von Mollard, J. Heberle, The DC gate in Channelrhodopsin-2: crucial hydrogen bonding interaction between C128 and D156, Photochem. Photobiol. Sci. 9 (2010) 194–198.
[30] A. Berndt, O. Yizhar, L.A. Gunaydin, P. Hegemann, K. Deisseroth, Bi-stable neural state switches, Nat. Neurosci. 12 (2009) 229–234.
[31] E.G. Govorunova, O.A. Sineshchekov, H. Li, Y. Wang, L.S. Brown, J.L. Spudich, RubyACRs, nonalgal anion channelrhodopsins with highly red-shifted absorption, Proc. Natl. Acad. Sci. U. S. A. 117 (2020) 22833–22840.
[32] S.A. Tennigkeit, R. Karapinar, T. Rudack, M.-A. Dreier, P. Althoff, D. Eickelbeck, T. Surdin, M. Grömmke, M.D. Mark, K. Spoida, M. Lübben, U. Höweler, S. Herlitze, K. Gerwert, Design of an ultrafast G protein switch based on a mouse melanopsin variant, Chembiochem 20 (2019) 1766–1771.
[33] A.A. Shtyrov, D.M. Nikolaev, V.N. Mironov, A.V. Vasin, M.S. Panov, Y.S. Tveryanovich, M.N. Ryazantsev, Simple models to study spectral properties of microbial and animal

rhodopsins: Evaluation of the electrostatic effect of charged and polar residues on the first absorption band maxima, Int. J. Mol. Sci. 22 (2021) 3029.
[34] K. Stehfest, E. Ritter, A. Berndt, F. Bartl, P. Hegemann, The branched photocycle of the slow-cycling channelrhodopsin-2 mutant C128T, J. Mol. Biol. 398 (2010) 690–702.
[35] O.A. Sineshchekov, E.G. Govorunova, H. Li, J.L. Spudich, Bacteriorhodopsin-like channelrhodopsins: Alternative mechanism for control of cation conductance, Proc. Natl. Acad. Sci. U. S. A. 114 (2017) E9512–E9519.
[36] S. Tajima, Y.S. Kim, M. Fukuda, Y. Jo, P.Y. Wang, J.M. Paggi, M. Inoue, E.F.X. Byrne, K.E. Kishi, S. Nakamura, C. Ramakrishnan, S. Takaramoto, T. Nagata, M. Konno, M. Sugiura, K. Katayama, T.E. Matsui, K. Yamashita, S. Kim, H. Ikeda, J. Kim, H. Kandori, R.O. Dror, K. Inoue, K. Deisseroth, H.E. Kato, Structural basis for ion selectivity in potassium-selective channelrhodopsins, Cell 186 (2023) 4325–4344.
[37] L.S. Brown, R. Needleman, J.K. Lanyi, Origins of deuterium kinetic isotope effects on the proton transfers of the bacteriorhodopsin photocycle, Biochemistry 39 (2000) 938–945.
[38] K. Inoue, S. Tahara, Y. Kato, S. Takeuchi, T. Tahara, H. Kandori, Spectroscopic study of proton-transfer mechanism of inward proton-pump rhodopsin, *Parvularcula oceani* Xenorhodopsin, J. Phys. Chem. B 122 (2018) 6453–6461.
[39] K. Shibata, K. Oda, T. Nishizawa, Y. Hazama, R. Ono, S. Takaramoto, R. Bagherzadeh, H. Yawo, O. Nureki, K. Inoue, H. Akiyama, Twisting and protonation of retinal chromophore regulate channel gating of channelrhodopsin C1C2, J. Am. Chem. Soc. 145 (2023) 10779–10789.
[40] F. Teufel, J.J. Almagro Armenteros, A.R. Johansen, M.H. Gíslason, S.I. Pihl, K.D. Tsirigos, O. Winther, S. Brunak, G. von Heijne, H. Nielsen, SignalP 6.0 predicts all five types of signal peptides using protein language models, Nat. Biotechnol. 40 (2022) 1023–1025.
[41] K.D. Tsirigos, C. Peters, N. Shu, L. Käll, A. Elofsson, The TOPCONS web server for consensus prediction of membrane protein topology and signal peptides, Nucleic Acids Res. 43 (2015) W401-7.
[42] J. Mähler, I. Persson, A study of the hydration of the alkali metal ions in aqueous solution, Inorg. Chem. 51 (2012) 425–438.
[43] Y.S. Kim, H.E. Kato, K. Yamashita, S. Ito, K. Inoue, C. Ramakrishnan, L.E. Fenno, K.E. Evans, J.M. Paggi, R.O. Dror, H. Kandori, B.K. Kobilka, K. Deisseroth, Crystal structure of the natural anion-conducting channelrhodopsin *Gt*ACR1, Nature 561 (2018) 343–348.
[44] A. Rozenberg, J. Oppermann, J. Wietek, R.G. Fernandez Lahore, R.-A. Sandaa, G. Bratbak, P. Hegemann, O. Béjà, Lateral gene transfer of anion-conducting channelrhodopsins between green algae and giant viruses, Curr. Biol. 30 (2020) 4910-4920.e5.
[45] A. Kianianmomeni, K. Stehfest, G. Nematollahi, P. Hegemann, A. Hallmann, Channelrhodopsins of *Volvox carteri* are photochromic proteins that are specifically expressed in somatic cells under control of light, temperature, and the sex inducer, Plant Physiol. 151 (2009) 347–366.
[46] R. Tashiro, K. Sushmita, S. Hososhima, S. Sharma, S. Kateriya, H. Kandori, S.P. Tsunoda, Specific residues in the cytoplasmic domain modulate photocurrent kinetics of channelrhodopsin from *Klebsormidium nitens*, Commun. Biol. 4 (2021) 235.
[47] M. Martin, Cutadapt removes adapter sequences from high-throughput sequencing reads, EMBnet.Journal 17 (2011) 10–12.
[48] D. Li, C.-M. Liu, R. Luo, K. Sadakane, T.-W. Lam, MEGAHIT: an ultra-fast single-node solution for large and complex metagenomics assembly via succinct de Bruijn graph, Bioinformatics 31 (2015) 1674–1676.

[49] W. Li, A. Godzik, Cd-hit: a fast program for clustering and comparing large sets of protein or nucleotide sequences, Bioinformatics 22 (2006) 1658–1659.
[50] L.S. Johnson, S.R. Eddy, E. Portugaly, Hidden Markov model speed heuristic and iterative HMM search procedure, BMC Bioinformatics 11 (2010) 431.
[51] V. Gradinaru, F. Zhang, C. Ramakrishnan, J. Mattis, R. Prakash, I. Diester, I. Goshen, K.R. Thompson, K. Deisseroth, Molecular and cellular approaches for diversifying and extending optogenetics, Cell 141 (2010) 154–165.

[52] N. Morimoto, T. Nagata, K. Inoue, Reversible photoreaction of a retinal photoisomerase, retinal G-protein-coupled receptor RGR, Biochemistry 62 (2023) 1429–1432.
[53] J.F. Fay, D.L. Farrens, Chapter fifteen - Purification of functional CB1 and analysis by site-directed fluorescence labeling methods, in: P.H. Reggio (Ed.), Methods in Enzymology, Academic Press, 2017: pp. 343–370.